Therapeutics, Targets, and Chemical Biology

Cancer Research

Antibody–Drug Conjugates Bearing Pyrrolobenzodiazepine or Tubulysin Payloads Are Immunomodulatory and Synergize with Multiple Immunotherapies

Jonathan Rios-Doria, Jay Harper, Raymond Rothstein, Leslie Wetzel, Jon Chesebrough, Allison Marrero, Cui Chen, Patrick Strout, Kathy Mulgrew, Kelly McGlinchey, Ryan Fleming, Binyam Bezabeh, John Meekin, David Stewart, Maureen Kennedy, Philip Martin, Andrew Buchanan, Nazzareno Dimasi, Emil Michelotti, and Robert Hollingsworth

Abstract

Immunogenic cell death (ICD) is the process by which certain cytotoxic drugs induce apoptosis of tumor cells in a manner that stimulates the immune system. In this study, we investigated whether antibody–drug conjugates (ADCS) conjugated with pyrrolobenzodiazepine dimer (PBD) or tubulysin payloads induce ICD, modulate the immune microenvironment, and could combine with immuno-oncology drugs to enhance antitumor activity. We show that these payloads on their own induced an immune response that prevented the growth of tumors following subsequent tumor cell challenge. ADCs had greater antitumor activity in immunocompetent versus immunodeficient mice, demonstrating a contribution of the immune system to the antitumor activity of these ADCs. ADCs also induced immunologic memory. In the CT26 model, depletion of $CD8^+$ T cells abrogated the activity of ADCs when used alone or in combination with a PD-L1 antibody, confirming a role for T cells in antitumor activity. Combinations of ADCs with immuno-oncology drugs, including PD-1 or PD-L1 antibodies, OX40 ligand, or GITR ligand fusion proteins, produced synergistic antitumor responses. Importantly, synergy was observed in some cases with suboptimal doses of ADCs, potentially providing an approach to achieve potent antitumor responses while minimizing ADC-induced toxicity. Immunophenotyping studies in different tumor models revealed broad immunomodulation of lymphoid and myeloid cells by ADC and ADC/immuno-oncology combinations. These results suggest that it may be possible to develop novel combinatorial therapies with PBD- and tubulysin-based ADC and immuno-oncology drugs that may increase clinical responses. *Cancer Res; 77(10); 2686–98. ©2017 AACR.*

Introduction

Cancer immunotherapy has revolutionized the way patients with cancer are being treated. Checkpoint inhibitor monoclonal antibodies against CTLA-4 and PD-1 have demonstrated clinical efficacy in multiple tumor types (1, 2). Several other immuno-oncology drugs are being developed that modulate both adaptive and innate immunity, and it has been hypothesized that combinatorial immuno-oncology strategies will provide more clinical benefit (3–5). Indeed, combinations of PD-1 and CTLA-4 antibodies have led to improved response rates and survival (6). However, there are still significant patient populations that do not respond to single-agent or immuno-oncology combinations. Many studies have focused on combining immuno-oncology drugs with cancer therapies that elicit immunogenic cell death (ICD) to improve response rates. ICD is the process whereby cells undergo apoptosis in a manner that results in the release of antigenic molecules that trigger an immune response (7). Radiation and certain chemotherapies, such as anthracyclines and oxaliplatin, induce ICD and combining liposomal doxorubicin with various immuno-oncology drugs led to synergistic antitumor responses in syngeneic mouse models (8–11). Targeted small-molecule therapeutics such as MEK and BRAF inhibitors have also been investigated in this regard, although it is not clear whether these agents induce ICD (12–15).

Recently, it has been hypothesized that combining immuno-oncology drugs with antibody–drug conjugates (ADC) could enhance antitumor responses and result in increased clinical benefit (16). ADCs combine the tumor-targeting specificity of an antibody with the potent cytotoxicity of small-molecule warheads, and this approach has been clinically validated with two ADCs currently marketed and an additional 50 being evaluated in clinical trials (17, 18). Certain ADC payloads have been identified that possess immunomodulatory activity. The maytansinoid ansamitocin P3 and dolastatins, from which auristatins are derived, induce dendritic cell maturation and secretion

MedImmune, Gaithersburg, Maryland.

Note: Supplementary data for this article are available at Cancer Research Online (http://cancerres.aacrjournals.org/).

Current address for D. Stewart: Glycomimetics, 9708 Medical Center Drive, Rockville, MD 20850.

Corresponding Author: Jonathan Rios-Doria, MedImmune, One MedImmune Way, Gaithersburg, MD 20878. Phone: 301-398-2867; Fax: 301-398-8580; E-mail: riosdoriaj@medimmune.com

doi: 10.1158/0008-5472.CAN-16-2854

of pro-inflammatory cytokines and increase T-cell priming and antitumor activity when combined with blockade of the PD-1/PD-L1 and CTLA-4 pathways (19, 20). In addition, a recent study has demonstrated that T-DM1, an FDA-approved ADC targeting $HER2^+$ tumors carrying the maytansine payload DM1, produced immune responses in patients with breast cancer treated in the clinic, and preclinically produced synergistic antitumor activity *in vivo* when combined with co-blockade of the CTLA-4 and PD-1 pathways (21). Taken together, these studies provide initial proof-of-concept that combining ADC and immuno-oncologys could produce strong antitumor effects.

In this report, we have investigated two additional ADC payload classes with varied mechanisms of action, pyrrolobenzodiazepines (PBD) and tubulysins, for their role in immunomodulation. PBDs are derivatives of naturally occurring antibiotics that bind in the minor groove of DNA forming inter- and intrastrand cross-linked adducts (22). Tubulysins are antimitotic agents that function to depolymerize microtubules (23). These compounds have been shown to be extremely potent as ADC payloads but little is known about their immunomodulatory functions (24, 25). Our studies reveal that both of these ADC payloads induce ICD, immunologic modulation and memory, and synergistic antitumor efficacy when combined with several different immunotherapies in mouse models.

Materials and Methods

Antibodies, reagents, and cell lines

All cell lines were obtained from ATCC except for the MCA205 cells, which were a gift from Andy Weinberg. CT26, 4T1, and MCA205 cells were grown in RPMI supplemented with 10% FBS. Renca cells were maintained in EMEM supplemented with 10% FBS. All cells were obtained between 2010 and 2013. Upon receipt, cell lines were re-authenticated using STR-based DNA profiling and multiplex PCR (IDEXX Bioresearch) and deposited in a central bank at MedImmune. PD-1 (RMP1-14), PD-L1 (10F.9G2), CD4 (GK1.5), and CD8 (53-6.7) antibodies were obtained from BioXCell. Mouse OX40 ligand fusion protein (OX40L FP) and mouse GITR ligand fusion protein (GITRL FP) were produced by MedImmune. To generate OX86 mIgG2a antibody, the OX86 hybridoma was purchased from Sigma (26). The Fc domain was then re-engineered to mouse IgG2a format by MedImmune (27). To generate the PD-L1 mIgG1 antibody, rats were immunized with recombinant mPDL1 Fc (R&D Systems #1019-B7). Rat lymph node samples were prepared and hybridomas established. Hybridoma supernatants were screened for binding to mPD-L1 protein using a Homogeneous Time Resolved Fluorescence assay, and clone 80 was selected on the basis of its desired specificity. Antibody variable genes were sequenced and the constant domain of the antibody exchanged to mouse IgG1 and expressed using a mammalian cell–based system. Anti-CTLA-4 antibody (9D9) was cloned and reformatted into a mouse IgG1 isotype (28). The anti-EphA2 antibody used in these studies has been previously described (29). The IGF1R antibody was generated via phage display selection using naïve human antibody libraries (30). Multiple rounds of phage display selection were performed using human and mouse IGF-1R extracellular domain (R&D Systems). ScFv specific for human and mouse IGF1R were converted to IgG and profiled.

Vaccination with warhead-treated cells

CT26 cells were treated with either 400 nmol/L methylmep-*N*-ethyl-tubulysinaniline (MMETA, tubulysin) or 8 nmol/L SG3199 (PBD) for 24 hours so that the cells were committed to cell death (as assessed by lack of growth in replating experiments) but still more than 95% viable. A total of 5×10^5 treated cells were inoculated into the right flank of BALB/c. Seven days later, 3×10^6 cells were implanted into the left flank. Controls included cells treated with 75-Gy radiation or taken through 3 freeze thaw cycles (necrotic).

AH1 restimulation assay

Spleens from mice that achieved complete response (CR) from ADC treatment were processed, and cells were plated at 2×10^6 cells per well in a 96-well plate. The cells were incubated with AH1 peptide (Anaspec #64798) at 10 μg/mL along with protein transport inhibitors (Ebioscience #00-4980-93) for 4 hours followed by evaluation by flow cytometry. The percentage of $CD45^+/CD8^+$ or $CD45^+/CD4^+$ that were also $TNF\alpha^+$ and/or $IFN\gamma^+$ were then analyzed.

Site-specific conjugation of warheads to generate ADCs

The PBD and tubulysin payloads were site specifically conjugated to cysteines engineered into the Fc domain of the antibodies. Reduced glycosylated reverse-phase HPLC (RP-HPLC) and liquid chromatography-mass spectrometry (LC-MS) were conducted to determine the drug:antibody ratio (DAR) and specificity of site-specific conjugation. These conjugation reactions produced ADCs with more than 98% monomer, with a conjugation efficiency of more than 90% correlating to a DAR >1.82.

In vivo efficacy studies

All *in vivo* studies were conducted in accordance to AAALAC and MedImmune IACUC guidelines for humane treatment and care of laboratory animals, and the general health of mice was monitored daily. Cells were cultured as monolayers, harvested by trypsinization, and implanted subcutaneously into either BALB/c, C57BL/6, or athymic nude mice (Envigo). For the CT26 and Renca tumor models, 5×10^5 cells were implanted in the right flank of 6- to 8-week-old female BALB/c mice. For the MCA205 tumor model, 2.5×10^5 cells were implanted in the right flank of 6- to 8-week-old female C57BL/6 mice. For the 4T1 tumor model, 1×10^5 cells were implanted in the right flank of 6- to 8-week-old female BALB/c mice. Intraperitoneal dosing of immuno-oncology drugs in the CT26 model was as follows: anti-PD-L1 (30 mg/kg, 2×/wk × 4); anti-PD-1 (20 mg/kg; 2×/wk × 4); mouse OX40 ligand fusion protein (5 mg/kg; 2×/wk × 2); mouse GITR ligand fusion protein (5 mg/kg; 2×/wk × 6). Dosing in the MCA205 model was as follows: mouse OX40L FP (20 mg/kg, 2×/wk × 2 doses). In the Renca model, EphA2-PBD was dosed at either 0.33 mg/kg, once a week for 3 doses or a single dose of 1 mg/kg. Mouse GITRL FP was dosed at 1 mg/kg, 2×/wk for 6 doses. The PD-L1 antibody used was clone 10F.9G2 unless otherwise specified. In the Renca model, anti-PD-L1 clone 80 and anti-CTLA-4 antibodies were dosed at 30 mg/kg, twice a week for four doses. ADCs were dosed by intravenous injection at 10 mL/kg of mouse body weight. Tumor and body weight measurements were collected twice weekly, and tumor volume was calculated using the equation $(L \times W^2)/2$, where L and W refer to the length and width dimensions, respectively. Error bars were calculated as SEM. At the beginning of treatment, mice were randomized by tumor

volume and were dosed when tumors reached 150 to 200 mm^3, with the exception of GITRL FP in the CT26 model, which was dosed when tumors reached about 300 mm^3.

Depletion studies

In the CT26 model, CD8 depleting antibody was administered (8 mg/kg) on days 6, 10, 14, and 18 after tumor cell implantation. EphA2-Tub was dosed at 5 mg/kg and EphA2-PBD was dosed at 0.3 mg/kg on day 11. Anti-PD-L1 was administered at 30 mg/kg on days 11, 14, 17, and 21. In the Renca model, CD4 and CD8 depleting antibodies were administered at 8 mg/kg on day 12, 15, 17, and 20. EphA2-PBD was dosed at 1 mg/kg on day 17.

Hematology studies

Naive 6- to 8-week-old BALB/c or C57Bl/6 mice were injected with EphA2-Tub (3 mg/kg) or EphA2-PBD (0.1 mg/kg). Blood was collected 1, 8, 15, and 22 post-dose. Lymphocyte counts were performed by Smithers Avanza. Blood samples were processed according to standard SOPs, and lymphocytes were counted using a Siemens Adiva 120 hematology analyzer.

Pharmacodynamic studies

CT26 cells (5×10^5 cells/mouse) were implanted in the right flank of 6- to 8-week-old BALB/c female mice. When tumors were about 150 to 200 mm^3, mice were dosed with EphA2-PBD (0.3 mg/kg), EphA2-Tub (5 mg/kg), anti-PDL1 (10F.9G2, 20 mg/kg), or OX40 monoclonal antibody (OX86, 5 mg/kg). ADCs were administered as one intravenous dose on day 0. PD-L1 antibody was administered on days 0, 4, 7, and 11, and OX40 antibody was administered on days 0 and 4. On day 5 and day 12 following dosing, spleen and tumor were collected, processed, and stained for flow cytometry. For the Renca model, EphA2-PBD was dosed at 1 mg/kg (single-dose) on day 0, when tumors were about 150 mm^3. GITRL FP was dosed on days 0 and 4, 7, and 11. Tumors were harvested on days 5 and 12. Red blood cells were lysed with ACK solution (Life Technologies). Tumors were cut into 2-mm^3 pieces and digested for 40 minutes using a Miltenyi Tumor Dissociation Human kit (Miltenyi Biotec). Tissues were counted for viability and then plated at 1 million cells per well. Live Dead Blue (Life Technologies) was stained at 1:1,000 for 20 minutes at room temperature and then washed and blocked using 4% mouse serum for 15 minutes at room temperature. Antibodies were added and then incubated at 4°C for 20 minutes in FACS buffer (PBS + 2% FBS). Cells were then washed, fixed, and permeabilized using a FOXP3 transcription kit (Ebioscience). Intracellular stains were applied for 30 minutes at room temperature. Cells were then washed and run on the LSRII or Fortessa Flow Cytometer (BD). Antibodies used for flow cytometric staining include CD8 (BD, Clone 5H10), CD11b (BD, Clone M1/70), CD4 (Biolegend Clone RM4-5), CD11c (Biolegend Clone n418), CD86 (Biolegend, Clone GL-1), GR-1 (Biolegend, Clone RB6-8C5), MHC-II (Biolegend Clone M5/114.15.2), F4/80 (Biolegend, Clone BM8), CD69 (Biolegend, Clone H1.2F3), Ki-67 (eBioscience, Clone SolA15), PD-1 (Ebioscience, Clone J43), FOXP3 (Ebioscience Clone FJK-16S), CD45 (eBioscience Clone 30-F11), TNF-α (Ebioscience Clone MP6-XT22, and IFN-γ (Clone XMG1.2). Data were analyzed using FlowJo software (Treestar). Normalized cell counts were calculated by dividing the total number of live cells in a gate by the total number of live and dead cells collected (non-debris) for each sample.

Flow cytometry for cell surface receptors

Adherent CT26, MCA205, 4T1, and Renca cells were removed with TrypLE Express, resuspended in complete medium, and then counted using a Vi-Cell XR Cell Viability Analyzer (Beckman Coulter). Cells were plated in duplicate in a round-bottom 96-well plate at 1×10^5 cells per well and centrifuged at $300 \times g$, 4°C for 4 minutes. Cell pellets were washed in FACS buffer (PBS + 2% FBS, 1 mmol/L EDTA) and again centrifuged. Cells were surface stained with 2.5 μg/mL of EphA2 antibody, 10 μg/mL of anti-IGFR1 antibody, or 2.5 μg/mL of isotype control antibody in FACS buffer for 30 minutes on ice. Cells were then washed 3 times in FACS buffer and resuspended in FACS buffer containing 5 μg/mL of goat-anti-human AlexaFluor 647 for 30 minutes on ice. Cells were washed 3 times and resuspended in FACS buffer containing 3 μmol/L DAPI. Data acquisition was performed with a MACSQuant VYB instrument (Miltenyi Biotec) and included forward and side scatter, DAPI using the V1 laser settings (violet: 405 nm; 40 mW; filter 450/50) and AlexaFluor 647 using the Y3 laser settings (yellow–green: 561 nm; 100 mW; filter 661/20). The photomultiplier tube (PMT) for the AlexaFluor 647 channel was kept constant per experiment.

Immunohistochemistry

Formalin-fixed, paraffin-embedded 5-μm-thick tumor sections were mounted on positively charged slides and stained. Slides were first deparaffinized in xylene and rehydrated using graded ethanol. Antigen unmasking was performed using Envision Flex Target Retrieval High pH 50x solution (Cat. no. K8000, Dako) in the Dako pressure cooker. Following antigen retrieval, slides were stained using an avidin biotin complex on a Dako Autostainer. Slides were stained with rat anti-mouse CD8a antibody (Cat. no. 14-0808-82, Ebioscience), followed by goat anti-rat biotin (Cat. no. 112-066-071, Jackson ImmunoResearch). After the stain, slides were counterstained with Mayer hematoxylin. EphA2 was detected with clone D4A2 (Cat. no. 6997S, Cell Signaling), followed by anti-rabbit secondary (Cat. no. K4003, Dako).

For $CD8^+$ cell quantitation, slides were scanned at 20× with an Aperio digital slide scanning system (Leica). Tumors were annotated using Aperio ImageScope (v12.2.2.5015) in two layers. Layer one consisted of the viable tumor regions. Layer two consisted of regions for exclusion from the analysis due to the presence of necrotic tissue, nonspecific background, or other tissue artifacts such as small folds. The annotated images were imported into Definiens Tissue Studio 4.1 using the Manual Region of Interest (ROI) Analysis Builder module. The analysis steps used the following analysis modules in sequence: manual ROI selection (draw polygons), initialize cellular analysis, nucleus detection, cell simulation, cell classification, and default export. The resulting analyzed images were quality-controlled by a board-certified ACVP pathologist (P. Martin), and the slides were analyzed with a semiquantitative scoring system (0 = none, 1 = minimal, 2 = mild, 3 = moderate, 4 = marked) to validate the results of the automated image analysis procedure.

Statistical analysis

Statistical analysis for synergy was determined using a Bliss independence model and described in detail elsewhere (8, 31). Differences between treatment groups in pharmacodynamic studies were determined using a 2-tailed Student *t* test. To appropriately power the combination studies, the number of animals per group was determined on the basis of sample size calculations using nQuery software.

Results

PBD- and tubulysin-treated cells can vaccinate against tumor challenge

It has been shown that antineoplastic compounds differ in their ability to induce ICD (11). To test whether tubulysin and PBD warheads could induce ICD, a vaccination/challenge assay, which is the gold-standard assay for identifying compounds that elicit ICD, was performed (7). CT26 cells were treated with either the tubulysin MMETA (400 nmol/L) or PBD SG3199 (8 nmol/L) for a period of 24 hours (Fig. 1A) such that the cells were still viable but committed to apoptosis. These dying cells were subcutaneously injected into BALB/c mice, followed by injection of live CT26 cells in the opposite flank 1 week later. Tubulysin- and PBD-treated cells provided vaccination and protected 40 and 70% of mice, respectively, from tumor formation when assessed on day 65 (Fig. 1B). As expected, necrotic cells did not vaccinate, as all re-challenged mice developed tumors, and vaccination with irradiated cells protected all mice from subsequent tumor rechallenge.

PBD- and tubulysin-conjugated ADCs trigger memory response

On the basis of these results, we investigated whether treatment of tumor-bearing mice with ADCs bearing tubulysin or PBD payloads could result in vaccination *in vivo*. For these studies, a murine cross-reactive antibody targeting EphA2 was utilized (29). Murine EphA2 was found to be overexpressed in several mouse carcinoma cell lines, including CT26, MCA205, 4T1, and Renca cells (Supplementary Fig. S1). This antibody was site specifically conjugated with a tubulysin (EphA2-Tub) or PBD (EphA2-PBD)

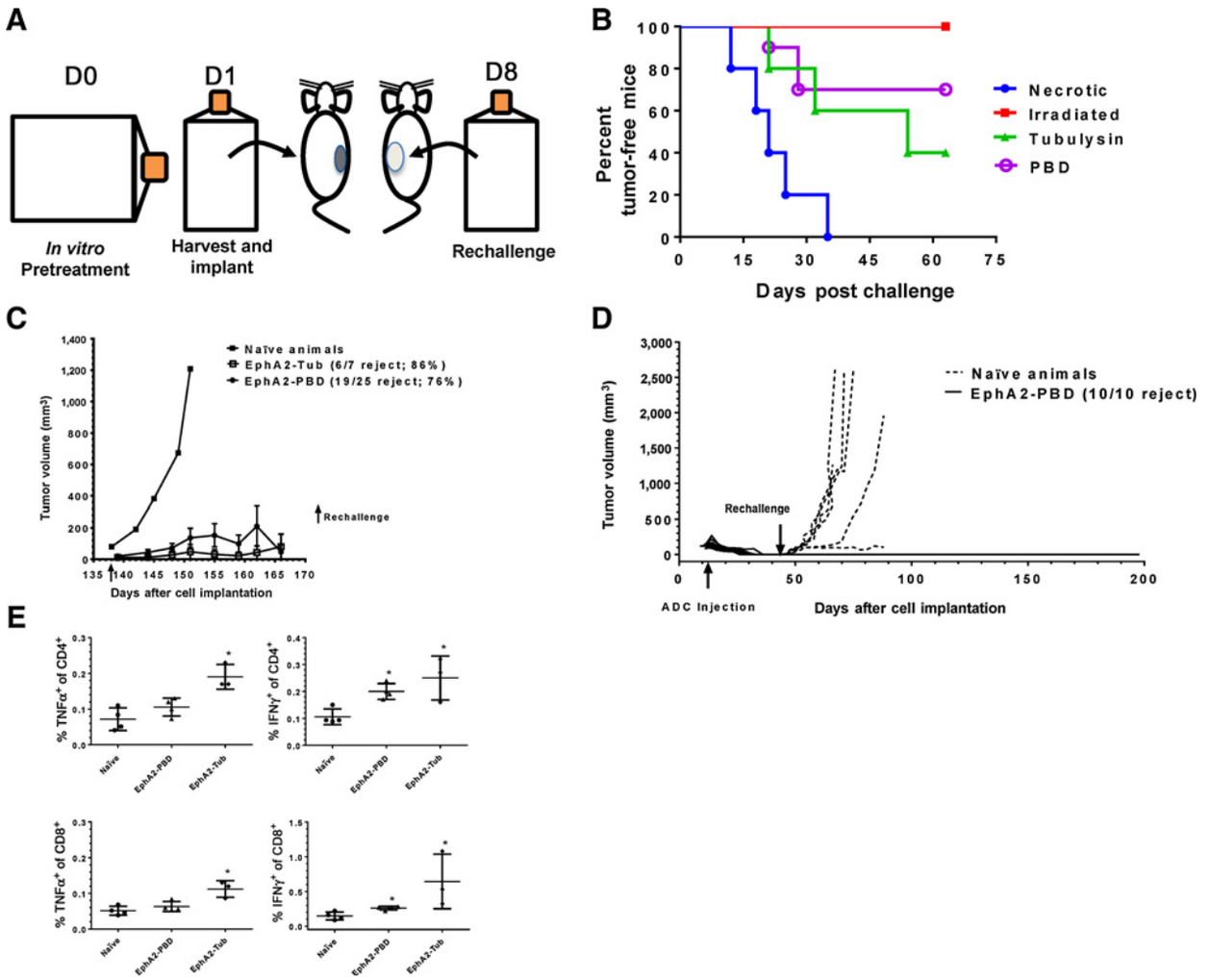

Figure 1.

Tubulysin and PBD warheads induce ICD and immunologic memory. **A,** Schematic representation of vaccination/challenge experiment. **B,** Percentage of tumor-free mice following rechallenge with live CT26 cells. **C,** Mean tumor volume following CT26 rechallenge in mice cured with either EphA2-Tub ADC or EphA2-PBD. **D,** Response of MCA205 tumors to EphA2-PBD (1 mg/kg) as well as growth of tumors rechallenged in either naïve or cured mice on day 43. **E,** Splenic T cells from naïve BALB/C mice or mice whose tumors were eradicated following treatment with either EphA2-Tub or EphA2-PBD (3–4 mice per group) were assayed for IFNγ and TNFα production following *ex-vivo* stimulation by the AH1 peptide. Top left, TNFα production in $CD45^+CD4^+$ cells; top right, IFNγ production in $CD45^+CD4^+$ cells; bottom left, TNFα production in $CD45^+CD8^+$ cells; bottom right, IFNγ production in $CD45^+CD8^+$ cells. *, $P < 0.05$ compared with untreated.

payload. CT26 tumor-bearing mice were administered multiple doses of these ADCs when average starting tumor volumes were either 75 or 150 mm^3. Each ADC produced a large percentage of CRs (Supplementary Table S1). Mice with CRs following treatment with either EphA2-PBD or EphA2-Tub were then re-challenged with CT26 cells 138 days after initial tumor challenge (Fig. 1C). Rejection of subsequent tumor rechallenge was high in mice that achieved CRs with ADC treatment: 86% and 76% of mice that achieved CRs with prior EphA2-Tub or EphA2-PBD treatment, respectively, remained tumor-free out to 166 days (Fig. 1C), whereas CT26 tumor growth was normal when simultaneously implanted in naïve mice. To ensure these effects were not model-specific, similar studies were conducted using the MCA205 syngeneic sarcoma model. A single 1-mg/kg dose of EphA2-PBD produced CRs in 10 of 10 MCA205 tumor–bearing mice (Fig. 1D). These mice were then rechallenged with MCA205 cells 43 days after initial challenge. All 10 mice rejected subsequent MCA205 rechallenge out to 190 days, whereas MCA205 cells grew normally in simultaneously injected naïve mice.

To determine whether T cells from mice cleared of CT26 tumors were functionally changed, splenic T cells were harvested and assayed for IFNγ and TNFα production following *ex-vivo* stimulation by the AH1 peptide; the immunodominant antigen of CT26 cells (32). In this assay, $CD4^+$ T cells from mice treated with EphA2-Tub produced TNFα upon stimulation with AH1 peptide (Fig. 1E, top left), whereas $CD4^+$ T cells from both EphA2-Tub- and EphA2-PBD–treated animals produced IFNγ (Fig. 1E, top right). A similar pattern of expression was found on $CD8^+$ T cells (Fig. 1E, bottom panels). These data demonstrate that PBD- and tubulysin-conjugated ADCs induced tumor-specific immunologic memory and generated T-cell populations that were functionally distinct from T cells from naïve mice.

T cells contribute to antitumor activity of ADCs

Given the observed immunomodulatory effects of these ADCs, studies were conducted to determine the contribution of the immune system on the antitumor activity of ADCs. We evaluated the antitumor activity of EphA2-ADCs against syngeneic tumor models grown in either T-cell–deficient (nude) mice or immunocompetent mice. CT26 (Fig. 2A), MCA205 (Fig. 2B), 4T1 (Fig. 2C), and Renca (Fig. 2D) tumors grown in either immunodeficient (left) or immunocompetent (right) mice were treated with either EphA2-Tub (top) or EphA2-PBD (bottom). As EphA2-Tub was relatively inactive in Renca tumor–bearing BALB/c mice (Supplementary Fig. S2), only EphA2-PBD was assessed in this setting. The reason for the lower activity of EphA2-Tub in the Renca model is likely due to the lower expression of EphA2 in this model (Supplementary Fig. S1D). In all four models, each ADC was more potent in immunocompetent mice compared with nude mice, which lack T cells, suggesting that T cells may be contributing to the ADC antitumor activity (Fig. 2). Additional experiments with control IgG ADCs demonstrated that the antitumor activity of EphA2 ADCs was EphA2 target–dependent in these models (Supplementary Fig. S3). To test whether T cells were contributing to antitumor activity, $CD8^+$ T cells were ablated from immunocompetent mice using a depleting anti-CD8 antibody. Strikingly, depletion of $CD8^+$ T cells abrogated the efficacy of the ADCs (Supplementary Fig. S4A). These data demonstrate that at the dose levels of ADCs used, $CD8^+$ T cells were required for full activity of EphA2-PBD and EphA2-Tub ADCs in the CT26 model.

Enhanced antitumor activity combining PBD or tubulysin conjugates with immuno-oncology drugs

That T cells contributed to ADC activity *in vivo* led to the hypothesis that antitumor activity could be enhanced by combining ADCs with T-cell modulating cancer immunotherapies. Before initiating combination studies with immuno-oncology drugs, we wished to examine the effect of EphA2-ADCs on the viability of lymphocytes in whole blood (Supplementary Fig. S5). When dosed at levels at or above those intended for combination studies, both EphA2-Tub and EphA2-PBD did decrease lymphocyte counts to a degree, however, levels rebounded by day 22, suggesting that acceptable levels of lymphocytes remained to be stimulated by immuno-oncology drugs. Compared with growth of untreated CT26 tumors (Fig. 3A), treatment with either EphA2-PBD or anti-PD-L1 resulted in 2 of 10 CRs in each group (Fig. 3B and C). However, the combination of EphA2-PBD and anti-PD-L1 administered concurrently produced a synergistic response with 7 of 10 CRs (Fig. 3D). Importantly, a suboptimal dose of EphA2-PBD (0.1 mg/kg) was used in this model. Strikingly, the enhanced activity of either ADC/anti-PD-L1 combination was almost completely abrogated following $CD8^+$ T-cell depletion (Supplementary Fig. S4B).

We then investigated combining these ADCs with an agonist to glucocorticoid-induced TNF receptor–related protein (GITR) using a mouse GITR ligand fusion protein (GITRL FP). GITRL/GITR interactions trigger T-cell activation and inhibit immunosuppression by regulatory T cells (T_{regs}) and thus GITR has been pursued as an immunotherapy target (33). Treatment of CT26-bearing mice with EphA2-Tub produced tumor growth delay but no CRs (Fig. 3E), whereas treatment with GITRL FP resulted in a potent antitumor response with 8 of 12 CRs observed (Fig. 3F). However, the combination of EphA2-Tub with GITRL FP dosed concurrently produced a profound synergistic response with CRs observed in all (12 of 12) mice (Fig. 3G).

Synergistic responses combining these ADCs with a PD-1 antibody or GITRL FP were also observed (Supplementary Table S2 and Supplementary Figs. S6 and S7). These results demonstrate that combining EphA2-ADCs carrying PBD or tubulysin payloads with checkpoint inhibitors or agonists of the TNFR superfamily results in potent antitumor effects *in vivo*.

Effects of ADCs and ADC/immuno-oncology combinations on T cells

Pharmacodynamic studies were conducted to determine the nature of the immunomodulatory effect of ADCs and ADC/immuno-oncology combinations. Immunophenotyping was carried out on CT26 tumors from mice treated with EphA2-PBD, EphA2-Tub, PD-L1 antibody, OX40 antibody, or combinations of these ADCs and immuno-oncology agents. EphA2-Tub induced an increase in the percent of intratumoral $CD45^+$ and $CD45^+CD8^+$ cells (Fig. 4A and B). With regard to $CD8^+$ cells, this increase was likely due to increased $CD8^+$ proliferation on the basis of an increase in $CD8^+Ki67^+$ cells observed with EphA2-tubulysin (Fig. 4C). While EphA2-PBD did not increase the overall percentage of intratumoral $CD8^+$ cells, this ADC along with EphA2-Tub increased the number of activated $CD8^+$ T cells, identified by an increase in the $CD8^+CD69^+$ population (Fig. 4D). Only OX40 mAb–treated groups decreased the percentage of $CD4^+$ cells and significantly depleted T_{regs} (Fig. 4E and F; ref. 27). Although EphA2-Tub increased $CD4^+FOXP3^+$ T_{regs} (Fig. 4E), the overall $CD8{:}T_{reg}$ ratio remained elevated compared with untreated CT26 tumors

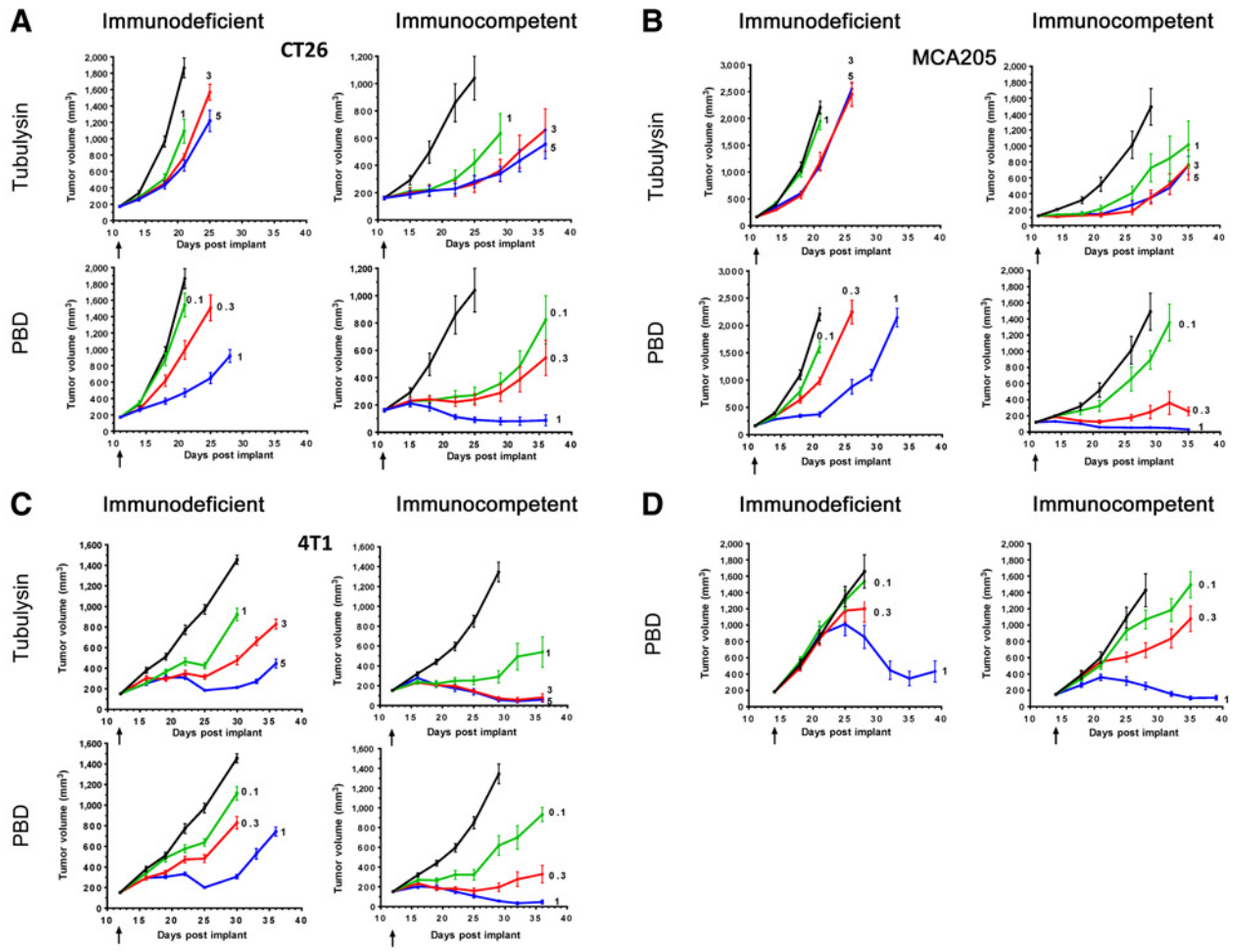

Figure 2.

Greater antitumor activity of ADCs in immunocompetent versus immunodeficient mice. The activity of EphA2-Tub (top) and EphA2-PBD (bottom) in immunodeficient (left) versus immunocompetent (right) mice was evaluated. **A,** CT26 tumor model. **B,** MCA205 tumor model. **C,** 4T1 tumor model. **D,** Renca tumor model. In all models, a single intravenous administration of ADC was given when the average tumor volume was 100 to 200 mm^3. The number in the graph indicates the dose of ADC in mg/kg that was administered. $n = 10$ per group.

(Fig. 4F). The CD8:T_{reg} ratio trended higher following EphA2-PBD treatment, although this was not statistically significant. Assessment of splenic cell populations revealed that combination of both ADCs with anti-PD-L1 and of EphA2-PBD with anti-OX40 increased the percent of $CD4^+PD\text{-}1^+$ cells, a marker of T-cell activation (Fig. 4H). A similar observation was made with these same groups in the induction of $CD4^+Ki67^+$ cells (Fig. 4I). These data suggest that activation and proliferation of splenic $CD4^+$ cells likely contributes to the larger effects of ADC/immuno-oncology combination compared with single-agent therapy.

$CD8^+$ T-cell tumor infiltration was also examined by immunohistochemistry (IHC). CT26 or MCA205 tumor–bearing mice were treated with EphA2-Tub or EphA2-PBD, and tumors were collected and stained for $CD8^+$ cells 2, 4, and 7 days after ADC administration (Fig. 5). Consistent with the FACS data, EphA2-Tub induced a gradual increase in $CD8^+$ cells (Fig. 5A). Quantification of these images demonstrated that EphA2-Tub induced a statistically significant increase in $CD8^+$ cells in the tumor at days 4 and 7 compared with a matched untreated sample taken on the same day (Fig. 5B). Again consistent with FACS (Fig. 4B), EphA2-PBD appeared to modestly increase $CD8^+$ cells compared with untreated tumors, but this did not result in statistical significance. In contrast, both EphA2-Tub and EphA2-PBD increased tumor-infiltrating $CD8^+$ cells in MCA205 tumors and to a larger degree than observed in CT26 tumors (Fig. 5C and D).

Effects of ADCs and ADC/immuno-oncology combinations on myeloid cells

EphA2-Tub alone and both ADCs in combination with anti-PD-L1 increased the percentage of $CD45^+CD86^+$ in the tumor (Fig. 6A). EphA2-Tub also increased the percentage of $F480^+CD86^+$ cells (Fig. 6B). All treatment groups increased the percentage of $CD86^+$ cells on mature dendritic cells, although the combination of EphA2-PBD with anti-OX40 and EphA2-Tub with anti-PD-L1 increased levels higher than single-agent therapy (Fig. 6C). Interestingly, EphA2-Tub induced tumor infiltration of $CD86^+$ granulocytic myeloid cells (Fig. 6D). In the spleen, modulation of CD86 on myeloid cell populations was found to be

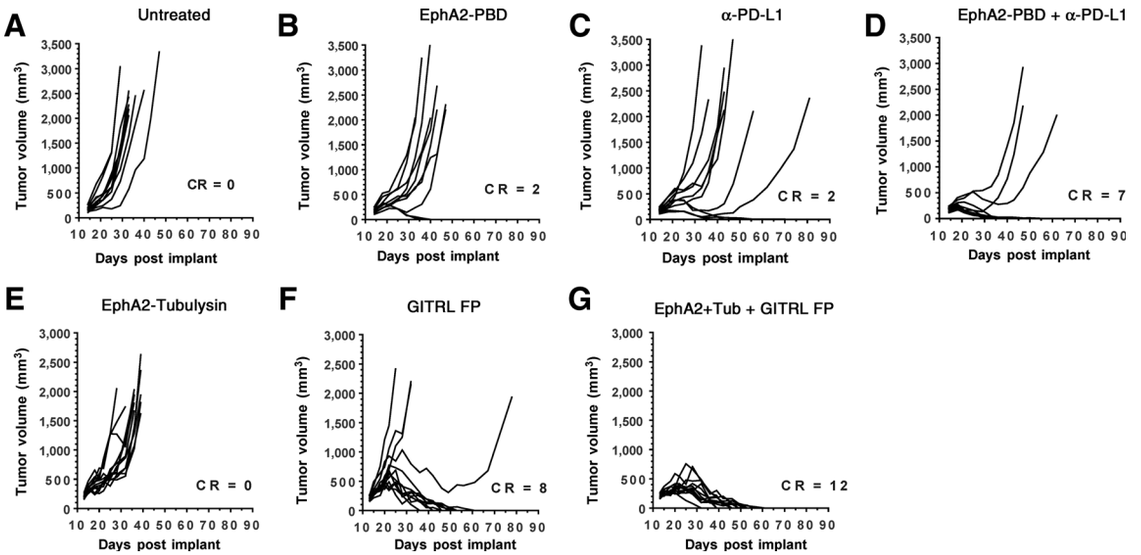

Figure 3.

Tubulysin and PBD ADCs synergize with immuno-oncology therapies. BALB/c mice bearing CT26 tumors were dosed with EphA2-PBD (0.1 mg/kg) or EphA2-Tub (3 mg/kg) alone or in combination with a PD-L1 antibody (30 mg/kg) or a mouse GITRL fusion protein (5 mg/kg). **A,** Untreated mice. **B,** EphA2-PBD. **C,** anti-PD-L1. **D,** EphA2-PBD + anti-PD-L1. **E,** EphA2-Tub. **F,** GITRL FP. **G,** EphA2-Tub + GITRL FP. CR frequency is out of 10 animals (α-PD-L1 combination) or out of 12 animals (GITRL FP combination).

significantly different in the combination versus single-agent groups. Both EphA2-PBD and EphA2-Tub in combination with anti-PD-L1 and EphA2-Tub in combination with anti-OX40 increased the percentage of $CD45^+CD86^+$ cells (Fig. 6E) A similar observation was found with these same groups and the induction of $F480^+CD86^+$ cells (Fig. 6F). Interestingly, both ADCs in combination with anti-PD-L1, but not with anti-OX40, increased the percentage of $CD11b^{hi}GR\text{-}1^{int}$ immature myeloid cells expressing CD86 in the spleen (Fig. 6G).

Similar effects with different ADCs or different models

While strong combination effects were obtained with ADCs targeting EphA2 in the CT26 model, we set out to determine whether this effect was target- and/or model-dependent. A murine cross-reactive antibody to the IGF1 receptor (IGF1R) was conjugated with PBD (IGF1R-PBD) and tested in the IGF1R-positive CT26 model (Supplementary Fig. S1E). CT26 tumor–bearing mice were dosed with IGF1R-PBD (Fig. 7A, top right), anti-PD-L1 (Fig. 7A, bottom left), and the combination (Fig. 7A, bottom right). Dramatic synergy was observed where all 12 of 12 mice achieved CRs in the combination group compared with one CR with IGF1R-PBD and four CRs with anti-PD-L1 treatment. These data provide evidence that the strong antitumor effects of combining ADCs with immunotherapy do not appear to be limited by the target antigen.

All of the data presented thus far have been using the CT26 model, which is known to be sensitive to many immunotherapies. We set out to determine whether ADCs can combine with immunotherapy in two other syngeneic models: MCA205 and Renca. EphA2-Tub combined with OX40L FP produced synergistic effects in the MCA205 model (Supplementary Fig. S8). As we previously observed enhanced activity of EphA2-PBD in Renca tumor–bearing immunocompetent compared with immunodeficient mice, we determined whether the activity of EphA2-PBD was dependent on $CD8^+$ T cells in this model. We also examined that the effect of combining EphA2-PBD with $CD4^+$ depletion as the Renca model was previously shown to be a T_{reg}-driven model, as depletion of T_{regs} via administration of various T_{reg}-depleting antibodies, including anti-CD4, resulted in tumor rejection (34). In contrast to the CT26 model, CD8 depletion had no effect on the growth of untreated tumors, nor on the antitumor activity of EphA2-PBD ADC (Supplementary Fig. S9A). CD4 depletion markedly inhibited tumor growth, consistent with a previous study (34). Surprisingly, EphA2-PBD in combination with CD4 depletion had a stronger antitumor effect than either CD4 depletion or EphA2-PBD alone (Supplementary Fig. S9A). These data suggested that the additional antitumor activity of the ADC in the presence of CD4 depletion may be due to loss of T_{regs}. GITR agonist antibodies and GITR ligand fusion proteins have been shown to deplete T_{regs} in mouse models (35, 36). In evaluating several different immunotherapies, Renca tumor–bearing mice were insensitive to anti-PD-L1 and anti-CTLA-4 but were sensitive to GITRL FP (Supplementary Fig. S9B; ref. 37). On the basis of these results, we examined the effects of combining EphA2-PBD with GITRL FP. Both EphA2-PBD (Fig. 7B, top right) and GITRL FP (Fig. 7B, bottom left) had minimal antitumor activity; however, the combination of EphA2-PBD and GITRL FP resulted in striking synergy and CRs in 9 of 10 animals (Fig. 7B, bottom right). Similar data were obtained when we used a fractionated ADC dose schedule instead of a single dose (Supplementary Fig. S9C).

Immunophenotyping of Renca tumors was examined both 5 and 12 days after administration of EphA2-PBD alone and in combination with GITRL FP. While the combination of EphA2-PBD and GITRL FP decreased the percentage of intratumoral $CD45^+$ cells at day 5, this percentage became larger by day 12 (Fig. 7C, top left). Importantly, EphA2-PBD alone also increased the percent of $CD45^+$ tumor-infiltrating lymphocytes (TIL) in the tumor at day 12. The percentage of $CD8^+$ cells was relatively unchanged at day 5 between all groups but was significantly higher following GITRL FP treatment alone and in combination

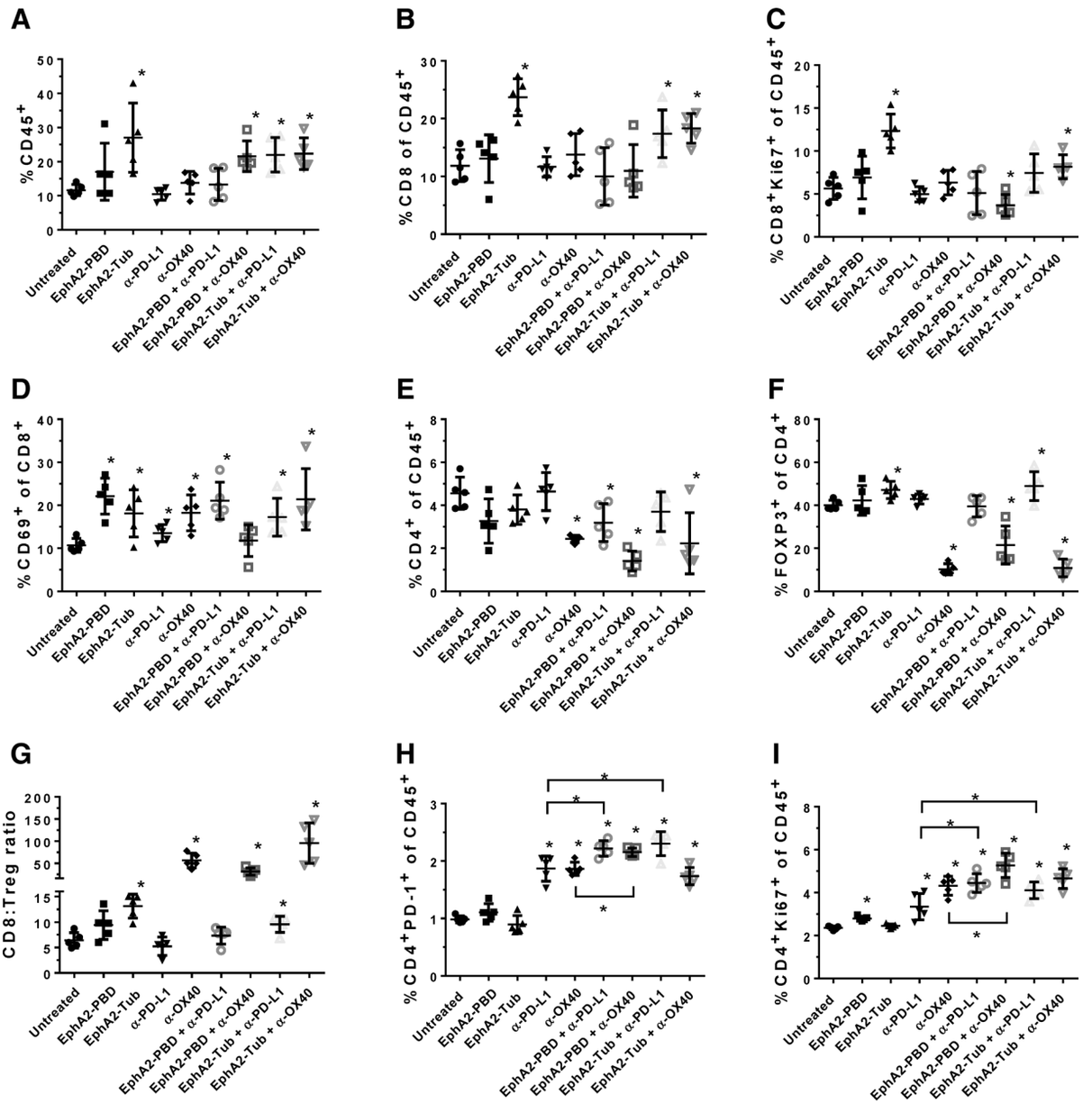

Figure 4.

Immunomodulatory effects of ADCs and ADC/immuno-oncology combinations in the CT26 model. CT26 tumor–bearing mice were treated with either EphA2-PBD or EphA2-Tub alone or in combination with either an OX40 or a PD-L1 antibody. Spleens and tumors were harvested 5 days after drug administration and flow cytometry was conducted using labeled antibodies against cell surface markers for various immune cell populations. **A,** Percentage of intratumoral $CD45^+$ leukocytes. **B,** Percentage of intratumoral $CD8^+$ of $CD45^+$ cells. **C,** Percentage of intratumoral $CD8^+Ki67^+$ of $CD45^+$ cells. **D,** Percentage of intratumoral $CD69^+$ of $CD8^+$ T cells. **E,** Percentage of intratumoral $CD4^+$ of $CD45^+$ cells. **F,** Percentage of intratumoral $FOXP3^+$ of $CD4^+$ cells. **G,** CD8:T_{reg} ratio in the tumor. **H,** Percentage of $CD4^+PD\text{-}1^+$ of $CD45^+$ cells in the spleen. **I,** Percentage of $CD4^+Ki67^+$ of $CD45^+$ cells in the spleen. *, $P < 0.05$ compared with untreated or bracketed group.

with EphA2-PBD (Fig. 7C, top right). All treatment groups transiently reduced the percentage of $CD4^+$ cells at day 5, which normalized at day 12 (Fig. 7C, bottom left). All treatment groups also transiently decreased the percentages of $CD4^+FOXP3^+$ T_{regs} at day 5, with the percentage of T_{regs} in the EphA2-PBD and GITRL FP combination significantly smaller than GITRL FP alone (Fig. 7C, bottom right).

As a fairly high dose of EphA2-PBD (1 mg/kg) was used in the Renca model, we also evaluated cell counts in response to treatment to determine whether ADC was affecting the numbers of $CD45^+$ cell populations in addition to modulating percentages. While the combination of EphA2-PBD and GITRL FP reduced the numbers of $CD45^+$ cells at day 5, the numbers rebounded by day 12 (Supplementary Fig. S10). Examination of

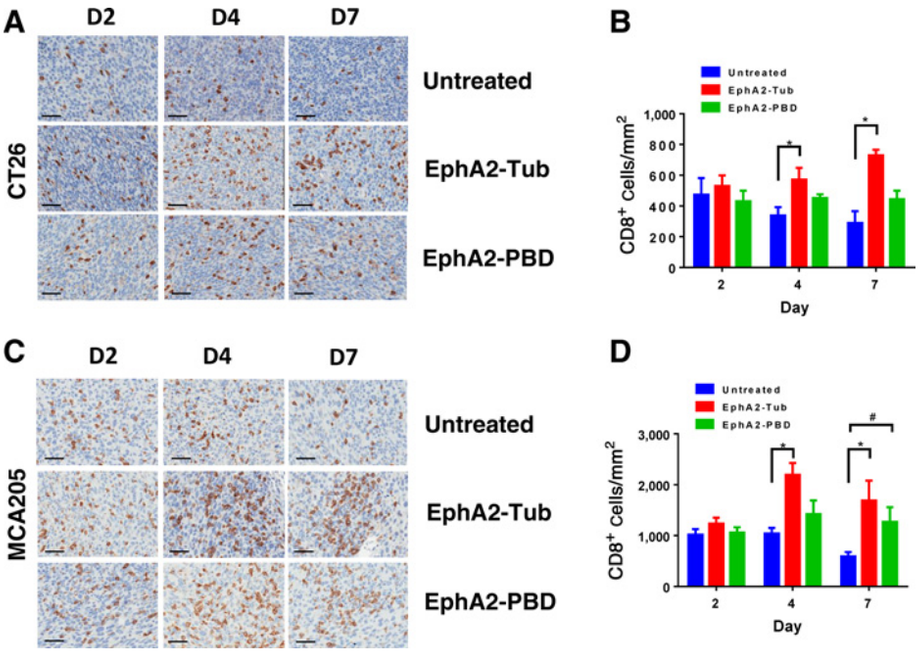

Figure 5.
$CD8^+$ T-cell tumor infiltration following ADC treatment. IHC of $CD8^+$ cells in CT26 or MCA205 tumors from mice treated with a single dose of EphA2-Tub (5 mg/kg) or EphA2-PBD (0.3 mg/kg). Animals were dosed when tumors were about 150 to 200 mm^3. Tumors were collected 2, 4, or 7 days after ADC administration. **A,** $CD8^+$ IHC of CT26 tumors. **B,** Quantification of images in **A**. **C,** $CD8^+$ IHC of MCA205 tumors. **D,** Quantification of images in **C**. Images are representative of 5 mice per group. Images were taken at 20×. Scale bar, 50 μm. *, $P < 0.05$; #, $P = 0.05$.

EphA2 expression with Renca tumors, as well as the other tumor models investigated in this study, demonstrated no detectable EphA2 expression in TILs, suggesting that the transient decrease in $CD45^+$ populations was due to bystander effect from the ADC (Supplementary Fig. S11). EphA2-PBD alone and in combination with GITRL FP transiently reduced the number of

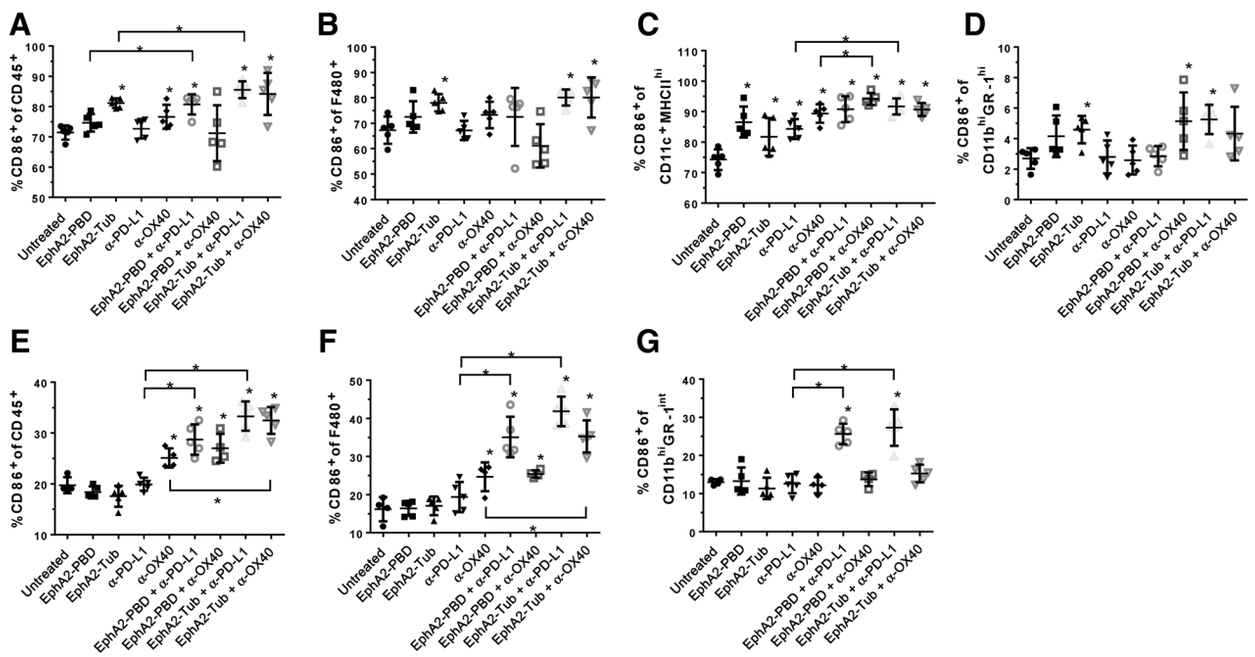

Figure 6.
Immunophenotyping of myeloid cell populations following ADC treatment in the CT26 model. CT26 tumor–bearing mice were treated with either EphA2-PBD or EphA2-Tub alone or in combination with an OX40 or an anti-PD-L1 antibody when tumors were about 300 mm^3. Tissue was collected either 5 days (tumor) or 12 days (spleen) after initial ADC dose. **A,** Percentage of $CD45^+CD86^+$ cells in the tumor. **B,** Percentage of $CD86^+$ of $F480^+$ macrophages in the tumor. **C,** Percentage of $CD86^+$ of $CD11c^+MHCII^{hi}$ cells in the tumor. **D,** Percentage of $CD86^+$ of $CD11b^{hi}GR\text{-}1^{hi}$ immature myeloid cells in the tumor. **E,** Percentage of $CD86^+$ of $F480^+$ macrophages in the spleen. **F,** Percentage of $CD86^+$ of $F480^+$ macrophages in the spleen. **G,** Percentage of $CD86^+$ of $CD11b^{hi}GR\text{-}^{hi}$ immature myeloid cells in the spleen. $n = 5$ per group. *, $P < 0.05$ compared to untreated or bracketed group.

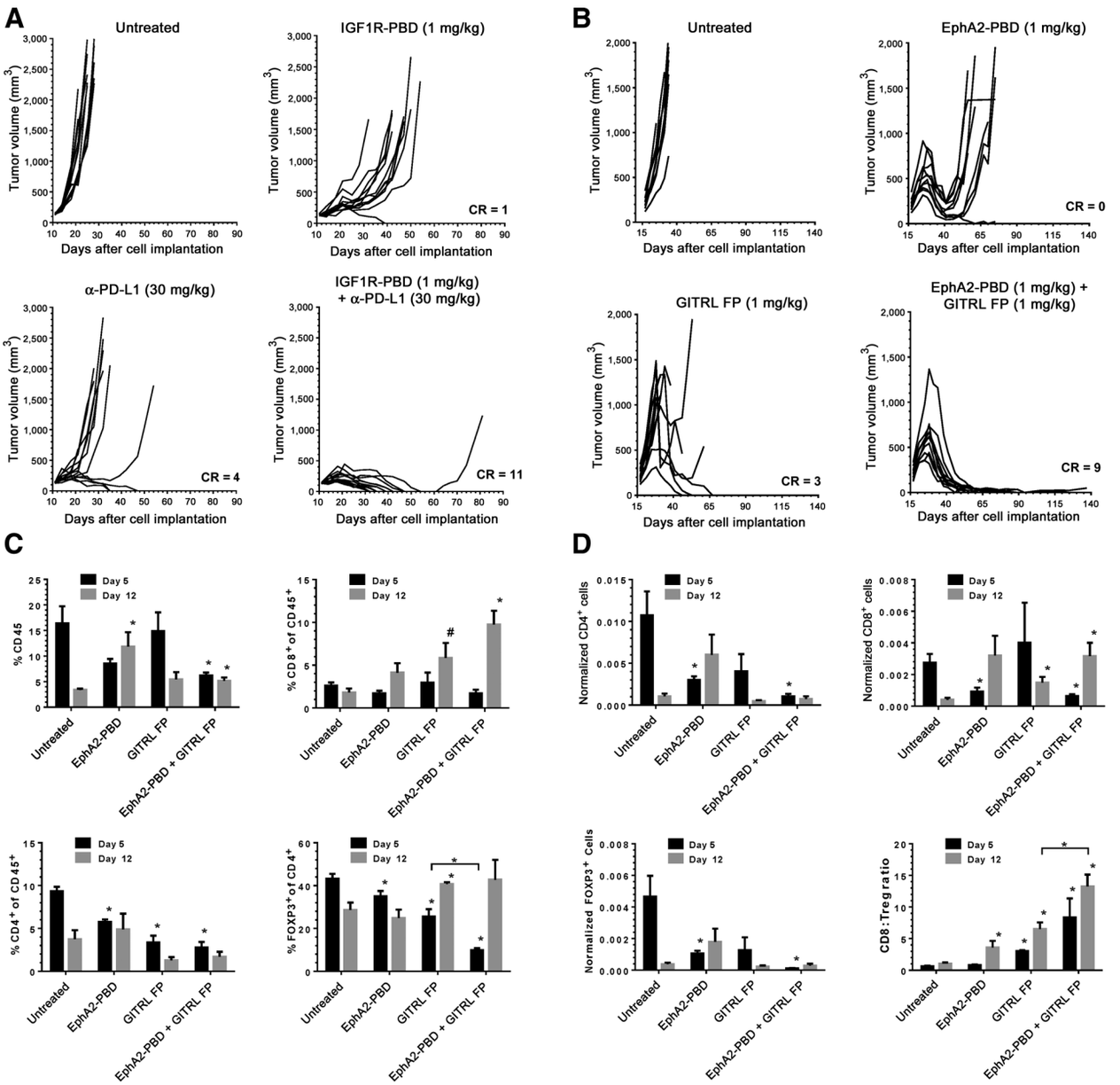

Figure 7.

Synergistic activity of ADC/immuno-oncology combinations is maintained when altering either the targeting antibody of the ADC or the syngeneic tumor model. **A,** Activity of IGF1R-PBD (top right), anti-PD-L1 (bottom left), or the combination (bottom right) in the CT26 model. CR observed (of 12 mice). **B,** Activity of EphA2-PBD (top right), GITR ligand fusion protein (bottom left), or the combination (bottom right) in the Renca model. CR observed (of 10 mice). Animals were dosed when tumors were about 150 to 200 mm^3. **C,** Immunophenotyping of Renca tumors by percentage. Top left, percentage $CD45^+$ cells; top right, percentage of $CD8^+$ of $CD45^+$ cells; bottom left, percentage $CD4^+$ of $CD45^+$ cells; bottom right, percentage of FOXP3 of $CD4^+$ cells. **D,** Immunophenotyping of Renca tumors by normalized cell count. Top left, normalized $CD4^+$ cells; top right, normalized $CD8^+$ cells; bottom left, normalized $FOXP3^+$ cells; bottom right, CD8:T_{reg} ratio. $N = 5$ animals per group. *, $P < 0.05$; #, $P = 0.05$ compared with untreated of equivalent day.

$CD4^+$ and $CD8^+$ cells at day 5, but these levels rebounded by day 12 (Fig. 7D, top left and right). GITRL FP alone and in combination with EphA2-PBD increased the number of intratumoral $CD8^+$ cells at day 12 (Fig. 7D, top right). Both EphA2-PBD and the EphA2-PBD/GITRL FP combination significantly decreased intratumoral T_{reg} numbers at day 5, with GITRL FP also trending to show a decrease (Fig. 7D, bottom left). The CD8:T_{reg} ratio of the GITRL FP and combination group increased at days 5 and 12 and also was observed with EphA2-PBD at day 12 (Fig. 7D, bottom right). Importantly, the CD8:T_{reg} ratio of the combination group was significantly higher than GITRL FP at day 12 (Fig. 7D, bottom right). Together, these data suggest that it is an increased CD8:T_{reg} ratio that drives the synergistic antitumor activity of the

combination of EphA2-PBD and GITRL FP. Examination of myeloid cells revealed that while EphA2-PBD decreased the percentage of $CD11c^{+}MHCII^{hi}$ mature dendritic cells in the tumor (Supplementary Fig. S12A), the majority of the remaining population was highly positive for CD80, which, like CD86, is a co-stimulatory molecule found on activated antigen-presenting cells (Supplementary Fig. S12B). The percentage of $F480^{+}CD80^{+}$ macrophages was also increased by EphA2-PBD and the combination (Supplementary Fig. S12C). These data suggest that EphA2-PBD is causing ICD *in vivo* and may contribute to the antitumor activity. Taken together, these similar results observed with multiple ADC combinations in multiple tumor models with varying levels of immune infiltrates suggest that these PBD- and tubulysin-based ADC/immuno-oncology combinations may provide clinical benefit in tumors with various immune phenotypes regardless of the targeting antibody of the ADC.

Discussion

In this report, we describe immunomodulation effects by three ADC payloads, PBD and tubulysin, and antitumor synergy of these ADCs upon combination with multiple cancer immunotherapies. Although PBD and tubulysin have distinct cytotoxic mechanisms of action, we found that both payloads were able to induce ICD and immunological memory. Mice whose tumors were cured with ADC treatment were vaccinated against subsequent tumor cell challenge in two different models. Although chemotherapy-induced ICD has previously been demonstrated for these tumor cell lines, this is the first report of such activity for these payloads (11, 38).

Our data point to two distinct mechanisms of action of the ADCs that results in increased efficacy in immunocompetent models. Data from the CT26 model demonstrated that $CD8^{+}$ T cells were directly induced by the ADCs and required for efficacy. This was associated with upregulation of costimulatory molecules, namely, CD86 in several myeloid populations, suggesting that ICD was being induced *in vivo*. In contrast, in the Renca model, it is likely the depletion of $T_{regs,}$ followed by a moderate increase in $CD8^{+}$ cells, and thus an increase in the $CD8{:}T_{reg}$ ratio, that accounts for the increased activity of EphA2-PBD. The transient depletion of T_{regs} in the Renca model is likely mediated through a bystander killing effect from the ADC payload as some of the bulk $CD4^{+}$ (as well as $CD8^{+}$) cells were transiently depleted in this model. Examination of tumor sections by IHC for EphA2 revealed no detectable EphA2 expression on TILs, ruling out that the antitumor activity of EphA2-PBD in the Renca model was due to target-mediated depletion of immunosuppressive cells. As the expression of EphA2 was lower in the Renca model than in others, a higher dose of EphA2-PBD (1 mg/kg) was required for activity, which may be the reason for the increased bystander killing in this model. An increase in $CD8{:}T_{reg}$ ratio induced by EphA2-PBD in the Renca model is seemingly in conflict with our data showing that depletion of $CD8^{+}$ cells has no effect on the activity of the ADC in this model. One explanation is that in the absence of $CD8^{+}$ cells, the tumor may be repopulated with other immunosuppressive cells, that the ADC is able to kill, resulting in increased tumor growth control.

It was reported recently that the ADC T-DM1 increased intratumoral $CD8^{+}$ and $CD4^{+}$ T cells, as well as $CD4^{+}FOXP3^{+}$ T_{regs}, and that T_{regs} were further increased by combining T-DM1 with PD1/CTLA4 blockade (21). In this model, TDM-1 treatment alone and in combination with anti-PD-1/CTLA-4 combination decreased the $CD8{:}T_{reg}$ ratio. In contrast, in our studies, we found that in 2 models, combining ADCs with immuno-oncology drugs increased the $CD8{:}T_{reg}$ ratios. With respect to PBD and tubulysin, our data highlight that at least in the models examined, increased $CD8{:}T_{reg}$ ratios may be a common driver of efficacy from ADC/immuno-oncology combinations. This suggests that differential modulation of $CD8^{+}$ cells and T_{regs} by ADCs may be model-dependent. It will be interesting to understand the effects of other Her-2–targeted ADCs, each containing different payloads, on immune cells in diverse patient populations (23, 39)

Examination of myeloid cell populations following treatment with ADCs revealed a frequent increase in CD86, a costimulatory molecule present on mature dendritic cells that is a marker of antigen-presenting cells (APC), as well as CD80 (40, 41). Interestingly, EphA2-Tub, and to a lesser degree EphA2-PBD, increased the percentage of $CD86^{+}$ granulocytic immature myeloid cells in CT26 tumors. Although the function of CD86 on immature myeloid cells remains poorly understood, it has previously been reported that docetaxel-induced upregulation of CD86 on immature myeloid cells reverses suppressive activity of myeloid-derived suppressor cells (MDSC; ref. 42). Another study reported that when loaded with a tumor antigen and an NKT ligand, immature myeloid cells could be converted to immunogenic APCs (43). Other studies have demonstrated reprogramming of immature myeloid cells, including MDSCs, to cell types that possess markers of mature dendritic cells following treatment of tumor-bearing mice with immunostimulatory agents (8, 42, 44). Increased antigen presentation of peripheral myeloid cells may play a key role in the enhanced activity of PBD- and tubulysin-based ADCs combined with immuno-oncology drugs.

ADC-induced toxicity is a problem that has been reported for several ADCs (45). Although meant to target tumors specifically, ADCs typically have off-target toxicities associated with payloads, and there are significant efforts to try to reduce the toxicities induced by ADCs (46, 47). It is noteworthy that enhanced activity with immuno-oncology agents in some of our studies was observed using subcurative doses of ADCs, in particular EphA2-PBD. However, doses that induced no antitumor activity did not enhance activity of immuno-oncology agents (data not shown). Our data suggest it is possible that by using suboptimal yet active doses of ADCs in combination with immuno-oncology agents, tolerability of ADCs may be improved. However, it will be critical to understand potential overlapping toxicities associated with ADCs and immuno-oncology agents to fully improve the therapeutic index.

This report describes the broad immunomodulating activities of two distinct ADC payloads, PBD and tubulysin, in multiple tumor models, using different ADC targets, and different and diverse immuno-oncology therapies. This is the first report of enhanced activity observed when combining immuno-oncology agents with ADCs conjugated with PBDs or tubulysins, and in addition, it is the first report of enhanced activity when combining ADCs with TNFR agonists. This is important, as many tumors are resistant to checkpoint blockade and may be sensitive to other classes of immunotherapies. The potent combination effects while targeting various tumor antigens in multiple tumor models with immuno-oncology agents of varying mechanisms of action suggests that different clinical tumor types may be candidates for treatment with ADC/immuno-oncology combinatorial therapies.

In summary, we believe that combining ADCs and immuno-oncology therapy represents a promising clinical strategy and may increase clinical responses and patient outcomes.

Disclosure of Potential Conflicts of Interest

R. Hollingsworth is the Senior Director of Oncology at MedImmune. No potential conflicts of interest were disclosed by the other authors.

Authors' Contributions

Conception and design: J. Rios-Doria, J. Harper, R. Rothstein, K. Mulgrew, R. Fleming, B. Bezabeh, N. Dimasi, E. Michelotti, R. Hollingsworth
Development of methodology: J. Harper, R. Rothstein, P. Strout, K. Mulgrew, R. Fleming, B. Bezabeh, D. Stewart, M. Kennedy, A. Buchanan, N. Dimasi, R. Hollingsworth
Acquisition of data (provided animals, acquired and managed patients, provided facilities, etc.): R. Rothstein, L. Wetzel, J. Chesebrough, A. Marrero, C. Chen, P. Strout, K. Mulgrew, K. McGlinchey, R. Fleming, B. Bezabeh, D. Stewart, P. Martin, A. Buchanan, N. Dimasi
Analysis and interpretation of data (e.g., statistical analysis, biostatistics, computational analysis): J. Rios-Doria, J. Harper, R. Rothstein, J. Chesebrough, K. Mulgrew, R. Fleming, B. Bezabeh, D. Stewart, P. Martin, N. Dimasi, E. Michelotti, R. Hollingsworth
Writing, review, and/or revision of the manuscript: J. Rios-Doria, J. Harper, L. Wetzel, J. Chesebrough, A. Marrero, A. Buchanan, N. Dimasi, E. Michelotti, R. Hollingsworth
Administrative, technical, or material support (i.e., reporting or organizing data, constructing databases): J. Rios-Doria, J. Harper, R. Rothstein, L. Wetzel, R. Fleming, B. Bezabeh, J. Meekin, D. Stewart
Study supervision: J. Rios-Doria, E. Michelotti, R. Hollingsworth
Other (*performed immunohistochemistry*): M. Kennedy
Other (*pathologist*): P. Martin

Acknowledgments

We thank Scott Hammond and Kris Sachsenmeier for insightful discussions. We thank Jessica Filderman for assistance with immunophenotypic studies. We also thank Holly Koelkebeck and Karma Dacosta for tissue and slide processing for the IHC studies. We thank Ronald Herbst for a critical review of this article. We thank Natalie Tigue and Lisa Bamber for the design and generation of the mouse GITRL FP and Claire Dobson, Jenny Percival-Alwyn, Jane Hammersley, Ling Huang, John Andrews, and Maria Groves for generation of the PD-L1 mIgG1 clone 80.

Grant Support

All studies were funded by MedImmune.

The costs of publication of this article were defrayed in part by the payment of page charges. This article must therefore be hereby marked *advertisement* in accordance with 18 U.S.C. Section 1734 solely to indicate this fact.

Received October 21, 2016; revised November 15, 2016; accepted March 2, 2017; published OnlineFirst March 10, 2017.

References

1. Callahan MK, Wolchok JD. At the bedside: CTLA-4- and PD-1-blocking antibodies in cancer immunotherapy. J Leukoc Biol 2013;94:41–53.
2. Wolchok JD, Kluger H, Callahan MK, Postow MA, Rizvi NA, Lesokhin AM, et al. Nivolumab plus ipilimumab in advanced melanoma. N Engl J Med 2013;369:122–33.
3. Khalil DN, Smith EL, Brentjens RJ, Wolchok JD. The future of cancer treatment: immunomodulation, CARs and combination immunotherapy. Nat Rev Clin Oncol 2016;13:394.
4. Smyth MJ, Ngiow SF, Ribas A, Teng MW. Combination cancer immunotherapies tailored to the tumour microenvironment. Nat Rev Clin Oncol 2016;13:143–58.
5. Hoos A. Development of immuno-oncology drugs - from CTLA4 to PD1 to the next generations. Nat Rev Drug Discov 2016;15:235–47.
6. Larkin J, Chiarion-Sileni V, Gonzalez R, Grob JJ, Cowey CL, Lao CD, et al. Combined nivolumab and ipilimumab or monotherapy in untreated melanoma. N Engl J Med 2015;373:23–34.
7. Kepp O, Senovilla L, Vitale I, Vacchelli E, Adjemian S, Agostinis P, et al. Consensus guidelines for the detection of immunogenic cell death. Oncoimmunology 2014;3:e955691.
8. Rios-Doria J, Durham N, Wetzel L, Rothstein R, Chesebrough J, Holoweckyj N, et al. Doxil synergizes with cancer immunotherapies to enhance antitumor responses in syngeneic mouse models. Neoplasia 2015;17:661–70.
9. Galluzzi L, Senovilla L, Zitvogel L, Kroemer G. The secret ally: immunostimulation by anticancer drugs. Nat Rev Drug Discov 2012;11:215–33.
10. Tesniere A, Schlemmer F, Boige V, Kepp O, Martins I, Ghiringhelli F, et al. Immunogenic death of colon cancer cells treated with oxaliplatin. Oncogene 2010;29:482–91.
11. Obeid M, Tesniere A, Ghiringhelli F, Fimia GM, Apetoh L, Perfettini JL, et al. Calreticulin exposure dictates the immunogenicity of cancer cell death. Nat Med 2007;13:54–61.
12. Liu L, Mayes PA, Eastman S, Shi H, Yadavilli S, Zhang T, et al. The BRAF and MEK inhibitors dabrafenib and trametinib: effects on immune function and in combination with immunomodulatory antibodies targeting PD-1, PD-L1, and CTLA-4. Clin Cancer Res 2015;21:1639–51.
13. Hu-Lieskovan S, Mok S, Homet Moreno B, Tsoi J, Robert L, Goedert L, et al. Improved antitumor activity of immunotherapy with BRAF and MEK inhibitors in BRAF(V600E) melanoma. Sci Transl Med 2015;7:279ra41.
14. Vanneman M, Dranoff G. Combining immunotherapy and targeted therapies in cancer treatment. Nat Rev Cancer 2012;12:237–51.
15. Sagiv-Barfi I, Kohrt HE, Czerwinski DK, Ng PP, Chang BY, Levy R. Therapeutic antitumor immunity by checkpoint blockade is enhanced by ibrutinib, an inhibitor of both BTK and ITK. Proc Natl Acad Sci U S A 2015;112:E966–72.
16. Gerber HP, Sapra P, Loganzo F, May C. Combining antibody-drug conjugates and immune-mediated cancer therapy: what to expect? Biochem Pharmacol 2016;102:1–6.
17. Schumacher D, Hackenberger CP, Leonhardt H, Helma J. Current status: site-specific antibody drug conjugates. J Clin Immunol 2016;36Suppl 1:100–7.
18. Thomas A, Teicher BA, Hassan R. Antibody-drug conjugates for cancer therapy. Lancet Oncol 2016;17:e254–62.
19. Muller P, Martin K, Theurich S, Schreiner J, Savic S, Terszowski G, et al. Microtubule-depolymerizing agents used in antibody-drug conjugates induce antitumor immunity by stimulation of dendritic cells. Cancer Immunol Res 2014;2:741–55.
20. Muller P, Martin K, Theurich S, von Bergwelt-Baildon M, Zippelius A. Cancer chemotherapy agents target intratumoral dendritic cells to potentiate antitumor immunity. Oncoimmunology 2014;3:e954460.
21. Muller P, Kreuzaler M, Khan T, Thommen DS, Martin K, Glatz K, et al. Trastuzumab emtansine (T-DM1) renders HER2+ breast cancer highly susceptible to CTLA-4/PD-1 blockade. Sci Transl Med 2015;7:315ra188.
22. Hartley JA. The development of pyrrolobenzodiazepines as antitumour agents. Expert Opin Investig Drugs 2011;20:733–44.
23. Li JY, Perry SR, Muniz-Medina V, Wang X, Wetzel LK, Rebelatto MC, et al. A biparatopic HER2-targeting antibody-drug conjugate induces tumor regression in primary models refractory to or ineligible for HER2-targeted therapy. Cancer Cell 2016;29:117–29.
24. Jeffrey SC, Burke PJ, Lyon RP, Meyer DW, Sussman D, Anderson M, et al. A potent anti-CD70 antibody-drug conjugate combining a dimeric pyrrolobenzodiazepine drug with site-specific conjugation technology. Bioconjug Chem 2013;24:1256–63.
25. Saunders LR, Bankovich AJ, Anderson WC, Aujay MA, Bheddah S, Black K, et al. A DLL3-targeted antibody-drug conjugate eradicates high-grade pulmonary neuroendocrine tumor-initiating cells*in vivo*. Sci Transl Med 2015;7:302ra136.
26. al-Shamkhani A, Birkeland ML, Puklavec M, Brown MH, James W, Barclay AN. OX40 is differentially expressed on activated rat and mouse T cells and is the sole receptor for the OX40 ligand. Eur J Immunol 1996;26:1695–9.

27. Bulliard Y, Jolicoeur R, Zhang J, Dranoff G, Wilson NS, Brogdon JL. OX40 engagement depletes intratumoral tregs via activating FcgammaRs, leading to antitumor efficacy. Immunol Cell Biol 2014; 92:475–80.
28. Peggs KS, Quezada SA, Chambers CA, Korman AJ, Allison JP. Blockade of CTLA-4 on both effector and regulatory T cell compartments contributes to the antitumor activity of anti-CTLA-4 antibodies. J Exp Med 2009; 206:1717–25.
29. Jackson D, Gooya J, Mao S, Kinneer K, Xu L, Camara M, et al. A human antibody-drug conjugate targeting EphA2 inhibits tumor growth*in vivo*. Cancer Res 2008;68:9367–74.
30. Lelliott CJ, Ahnmark A, Admyre T, Ahlstedt I, Irving L, Keyes F, et al. Monoclonal antibody targeting of fibroblast growth factor receptor 1c ameliorates obesity and glucose intolerance via central mechanisms. PLoS One 2014;9:e112109.
31. Zhao W, Sachsenmeier K, Zhang L, Sult E, Hollingsworth RE, Yang H. A new bliss independence model to analyze drug combination data. J Biomol Screen 2014;19:817–21.
32. Rice J, Buchan S, Stevenson FK. Critical components of a DNA fusion vaccine able to induce protective cytotoxic T cells against a single epitope of a tumor antigen. J Immunol 2002;169:3908–13.
33. Schaer DA, Murphy JT, Wolchok JD. Modulation of GITR for cancer immunotherapy. Curr Opin Immunol 2012;24:217–24.
34. Teng MW, Swann JB, von Scheidt B, Sharkey J, Zerafa N, McLaughlin N, et al. Multiple antitumor mechanisms downstream of prophylactic regulatory T-cell depletion. Cancer Res 2010;70:2665–74.
35. Coe D, Begom S, Addey C, White M, Dyson J, Chai JG. Depletion of regulatory T cells by anti-GITR mAb as a novel mechanism for cancer immunotherapy. Cancer Immunol Immunother 2010;59: 1367–77.
36. Schaer DA, Budhu S, Liu C, Bryson C, Malandro N, Cohen A, et al. GITR pathway activation abrogates tumor immune suppression through loss of regulatory T cell lineage stability. Cancer Immunol Res 2013;1: 320–31.
37. Hu P, Arias RS, Sadun RE, Nien YC, Zhang N, Sabzevari H, et al. Construction and preclinical characterization of fc-mGITRL for the immunotherapy of cancer. Clin Cancer Res 2008;14:579–88.
38. Casares N, Pequignot MO, Tesniere A, Ghiringhelli F, Roux S, Chaput N, et al. Caspase-dependent immunogenicity of doxorubicin-induced tumor cell death. J Exp Med 2005;202:1691–701.
39. Ogitani Y, Aida T, Hagihara K, Yamaguchi J, Ishii C, Harada N, et al. DS-8201a, A novel HER2-targeting ADC with a novel DNA topoisomerase I inhibitor, demonstrates a promising antitumor efficacy with differentiation from T-DM1. Clin Cancer Res 2016;22:5097–108.
40. Konermann A, Deschner J, Allam JP, Novak N, Winter J, Baader SL, et al. Antigen-presenting cell marker expression and phagocytotic activity in periodontal ligament cells. J Oral Pathol Med 2012;41:340–7.
41. McLellan AD, Starling GC, Williams LA, Hock BD, Hart DN. Activation of human peripheral blood dendritic cells induces the CD86 co-stimulatory molecule. Eur J Immunol 1995;25:2064–8.
42. Kodumudi KN, Woan K, Gilvary DL, Sahakian E, Wei S, Djeu JY. A novel chemoimmunomodulating property of docetaxel: suppression of myeloid-derived suppressor cells in tumor bearers. Clin Cancer Res 2010; 16:4583–94.
43. Lee JM, Seo JH, Kim YJ, Kim YS, Ko HJ, Kang CY. The restoration of myeloid-derived suppressor cells as functional antigen-presenting cells by NKT cell help and all-trans-retinoic acid treatment. Int J Cancer 2012;131:741–51.
44. Holmgaard RB, Brachfeld A, Gasmi B, Jones DR, Mattar M, Doman T, et al. Timing of CSF-1/CSF-1R signaling blockade is critical to improving responses to CTLA-4 based immunotherapy. Oncoimmunology 2016;5: e1151595.
45. Gorovits B, Krinos-Fiorotti C. Proposed mechanism of off-target toxicity for antibody-drug conjugates driven by mannose receptor uptake. Cancer Immunol Immunother 2013;62:217–23.
46. Hinrichs MJ, Dixit R. Antibody drug conjugates: nonclinical safety considerations. AAPS J 2015;17:1055–64.
47. Donaghy H. Effects of antibody, drug and linker on the preclinical and clinical toxicities of antibody-drug conjugates. MAbs 2016;8:659–71.